

Dynamic signatures of the transition from stacking disordered to hexagonal ice: Dielectric and nuclear magnetic resonance studies

C. Gainaru, E. Vynokur, K. W. Köster, V. Fuentes-Landete, N. Spettel, J. Zollner, T. Loerting, and R. Böhmer

Citation: *The Journal of Chemical Physics* **148**, 134502 (2018); doi: 10.1063/1.5023178

View online: <https://doi.org/10.1063/1.5023178>

View Table of Contents: <http://aip.scitation.org/toc/jcp/148/13>

Published by the [American Institute of Physics](#)

Articles you may be interested in

Comment on “The putative liquid-liquid transition is a liquid-solid transition in atomistic models of water” [I and II: *J. Chem. Phys.* 135, 134503 (2011); *J. Chem. Phys.* 138, 214504 (2013)]

The Journal of Chemical Physics **148**, 137101 (2018); 10.1063/1.5029463

Ice nucleation rates near ~ 225 K

The Journal of Chemical Physics **148**, 084501 (2018); 10.1063/1.5019362

Relaxation dynamics and transformation kinetics of deeply supercooled water: Temperature, pressure, doping, and proton/deuteron isotope effects

The Journal of Chemical Physics **147**, 034506 (2017); 10.1063/1.4993790

Potential energy landscape of TIP4P/2005 water

The Journal of Chemical Physics **148**, 134505 (2018); 10.1063/1.5023894

Microscopic structural descriptor of liquid water

The Journal of Chemical Physics **148**, 124503 (2018); 10.1063/1.5024565

The barrier to ice nucleation in monatomic water

The Journal of Chemical Physics **148**, 124505 (2018); 10.1063/1.5016518

PHYSICS TODAY

WHITEPAPERS

ADVANCED LIGHT CURE ADHESIVES

Take a closer look at what these environmentally friendly adhesive systems can do

READ NOW

PRESENTED BY
 MASTERBOND
ADHESIVES | SEALANTS | COATINGS

Dynamic signatures of the transition from stacking disordered to hexagonal ice: Dielectric and nuclear magnetic resonance studies

C. Gainaru,^{1,a)} E. Vynokur,¹ K. W. Köster,¹ V. Fuentes-Landete,² N. Spettel,² J. Zollner,² T. Loerting,² and R. Böhmer¹

¹Fakultät Physik, Technische Universität Dortmund, D-44221 Dortmund, Germany

²Institute of Physical Chemistry, University of Innsbruck, A-6020 Innsbruck, Austria

(Received 22 January 2018; accepted 13 March 2018; published online 2 April 2018)

Using various temperature-cycling protocols, the dynamics of ice I were studied via dielectric spectroscopy and nuclear magnetic resonance relaxometry on protonated and deuterated samples obtained by heating high-density amorphous ices as well as crystalline ice XII. Previous structural studies of ice I established that at temperatures of about 230 K, the stacking disorder of the cubic/hexagonal oxygen lattice vanishes. The present dielectric and nuclear magnetic resonance investigations of spectral changes disclose that the memory of the existence of a precursor phase is preserved in the hydrogen matrix up to 270 K. This finding of hydrogen mobility lower than that of the undoped hexagonal ice near the melting point highlights the importance of dynamical investigations of the transitions between various ice phases and sheds new light on the dynamics in ice I in general. *Published by AIP Publishing.* <https://doi.org/10.1063/1.5023178>

I. INTRODUCTION

The transition between stacking disordered (in the following for simplicity called cubic) and hexagonal ices has been receiving particular attention due to its implication on Earth's atmosphere. Cubic ice (ice I_c) is a rather peculiar form of ice which can be produced at ambient pressure upon heating the amorphous and the high-pressure crystalline ices toward the thermodynamical habitat of hexagonal ice (ice I_h). Ice I_c is generally considered to be a metastable polytypic form of stable hexagonal ice which differs from it in terms of the stacking sequence. Starting with the observation of Scheiner's halo in 1629, claims were made about the occasional existence of cubic ice crystals in clouds,^{1–3} e.g., in noctilucent mesospheric or polar stratospheric clouds. These claims are being debated since also polycrystals of hexagonal ice^{4,5} or trigonal crystals may be of relevance in this context.⁶ The higher vapor pressure and the lower thermal conductivity⁷ of ice I_c as compared to ice I_h might be of importance in cloud freezing and persistent in-cloud supersaturations in cold cirrus.⁸ Ultimately, larger crystals of ice I_h might form via ice I_c , thereby more efficiently dehydrating air.⁹ Irrespective of the controversy related to atmospheric clouds, it is generally accepted that ice I_c plays an important role in astrophysical environments, such as on comets approaching the sun.^{10,11}

At variance with the situation for ice I_h (space group $P6_3/mmc$), it has so far not been possible to grow a large single crystal of ice I_c (space group $Fd\bar{3}m$). All known forms of cubic ice contain a more or less significant amount of

hexagonal stacking sequences, depending on the details of preparation, most notably upon the mother phase ice I_c was produced from Ref. 12. Thus, it was proposed to rename cubic ice as stacking-disordered ice I_{sd} (space group $P3m1$)¹³ or ice I_{ch} , mirroring the presence of both cubic and hexagonal stacking.¹² The higher the temperature, the less cubic stacking is found in ice I in general, and so it was suggested to depict the change in stacking sequence with increasing temperature as ice $I_{c(h)} \rightarrow I_{ch} \rightarrow I_{(c)h} \rightarrow I_h$.¹² In order to describe this transition, more rigorously “cubicity” of ice I_c was defined.¹⁴ In early calorimetry work, this complex transformation kinetics process was shown to take place continuously.¹⁵ Depending on the mother phase, the initial and the final temperatures for the cubic to hexagonal ice conversion were reported to vary between 175–191 K and 217–233 K, respectively.¹⁵ This transition was shown to proceed in two steps, a faster release of heat of width 16 K, followed by a slow release that was observed up to rather high temperatures, increasing the overall width to about 54 K.¹⁵ Thus, the cubic to hexagonal transition is much broader than other polymorphic transitions in ice. The gradual nature of the transformation was noticed quite early.^{16,17} Its underlying mechanism was recently suggested to involve motion of partial dislocations in fine-grained, polycrystalline ice with a high density of widely extended dislocations.¹⁸ Cubicity of hexagonal ice was noticed at temperatures even higher than 233 K: For instance, ice I_c produced from other mother phases such as gas hydrates or amorphous ice transforms fully to hexagonal ice only near 240 K.¹⁹ Furthermore, ice I_c produced from liquid water near 250 K²⁰ and water frozen in solid inclusions was shown to contain cubic stacking sequences up to 258 K.¹³

In all these examples, ice I_c is favored at lower temperatures, whereas ice I_h dominates at higher temperatures.

^{a)}E-mail: catalin.gainaru@uni-dortmund.de

The transformation to ice I_h is usually considered to be complete much below the melting point T_m , with cubic stacking sequences presumed to play no role near T_m . These conclusions are based on results from vibrational spectroscopy^{21–23} or structural methods,^{11–14,20,24–29} especially diffraction.

Much less information is available for cubic ice from techniques focusing on hydrogen dynamics. Time constants in the range from 10^4 to 10^6 s have been reported on the basis of temperature drift measurements.³⁰ They were found to be consistent with dielectric data in the seconds range³¹ but much longer than the time constants for hexagonal ice using enthalpy relaxation.³² As far as we know, dynamical aspects of the transition toward neat hexagonal ice have so far not been addressed with this type of spectroscopy. In the present work, we investigate the corresponding dielectric response in the range from 0.1 Hz to 100 kHz. Nuclear magnetic resonance (NMR) relaxometry studies of the $I_{c(h)} \rightarrow I_h$ transition which probe the dynamics typically on the 10–100 MHz scale are also scarce,³³ and such experiments were also conducted in the present work. Here we show that the *dynamical* fingerprints corresponding to the conversion to hexagonal phase survive at much higher temperatures than previously anticipated. These results are based on a comparison of dynamic investigations (NMR and dielectric relaxation spectroscopy) of cubic ice produced from different initial phases, specifically expanded and unrelaxed high-density amorphous ice (eHDA and uHDA, respectively), and from crystalline ice XII.

II. EXPERIMENTAL DETAILS

Dielectric spectra were acquired using a Novocontrol system including an Alpha impedance analyzer and a Quatro temperature controller. The mother phases for the cubic ice samples studied in the present work are low-density amorphous ice (LDA) and ice XII. The samples initially prepared as high-density amorphous ices (uHDA and eHDA) and ice XII were smashed into powders and transferred to an invar/sapphire cell at liquid nitrogen temperature as previously described.³⁴ Due to uncertainties in the filling factor of the cell, the amplitude of the dielectric losses is presented in arbitrary units. Prior to spectra acquisition, temperature was equilibrated for about 20 min to achieve a stability level of 0.1 K. The samples were investigated as protonated and as deuterated materials to allow for better comparability with results from ^2H NMR and to check for isotope effects on the dynamics of hydrogen matrix. For the NMR measurements the samples were cold loaded into glass tubes that were subsequently sealed. Immersed in liquid nitrogen the tubes were inserted in the sample coil of the probe head which was then transferred into a cryostat precooled to 77 K. Deuteron NMR spin-lattice relaxation experiments were conducted at a Larmor frequency of $\omega_L = 2\pi \times 55$ MHz by applying the saturation recovery technique and recording the longitudinal magnetization recoveries; see Ref. 35 for further details.

The initial uHDA/ H_2O sample was prepared as originally described by Mishima *et al.*,³⁶ specifically by compressing 600 mg of hexagonal ice at 77 K to 1.6 GPa. The initial eHDA/ H_2O and eHDA/ D_2O samples were prepared as

described by Amann-Winkel *et al.*³⁴ Specifically, first uHDA was produced, which was then converted to very-high-density amorphous (VHDA) ice by heating to 165 K at 1.1 GPa, followed by conversion to eHDA through decompression to 0.1 GPa at 140 K (H_2O) and 143 K (D_2O), respectively. The LDA mother phases were obtained both from uHDA and eHDA after quench-recovery to 77 K and 1 bar inside the sample holders used for dielectric and NMR experiments. This was achieved by heating the HDA samples at 1 bar through the polyamorphic transition to LDA, which occurs at about 110 K (uHDA) or 130 K (eHDA). Please note that a very small difference in the intermediate range ordering was noted between these two LDA forms.³⁷ Ices XII/ H_2O and XII/ D_2O were prepared by crystallizing uHDA at fast rates and high pressures. Specifically, 600 mg of uHDA were heated at >25 K/min from 77 K to beyond the crystallization temperature at 0.81 GPa to 200 K. The use of high rates is essential to avoid ice IV as by-phase of the crystallization.³⁸

The purity of all phases initially prepared was checked by means of powder X-ray diffraction at ~ 80 K using a Siemens D5000 diffractometer and an Anton-Paar low-temperature chamber.

III. EXPERIMENTAL RESULTS AND ANALYSES

A. Dielectric spectroscopy

Using dielectric spectroscopy performed in a standard mode, e.g., in a simple upward or a simple downward temperature scan, a straightforward dielectric signature of a transition

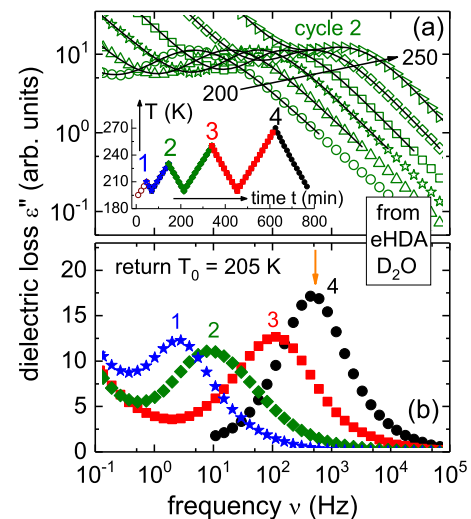


FIG. 1. (a) Dielectric loss spectra of ice I obtained from deuterated eHDA. The measurements were taken from 200 to 250 K in steps of 10 K. The solid lines are fits using Eq. (1); see the text for details. The inset shows the employed temperature cycling scheme. Spectra are shown for the second cycle. The scan rate was $|dT/dt| = 0.4$ K/min. For each cycle, the minimum and the maximum temperatures are the return temperature T_0 and the peak temperature T_p , respectively. The numbers 1, 2, 3, and 4 mark the beginnings of each temperature cycle, and for eHDA/ D_2O they correspond to $T_p = 210, 230, 250,$ and 270 K, respectively. (b) Loss measurements carried out at $T_0 = 205$ K after each cycle, i.e., after cooling down ice I obtained from deuterated eHDA from T_p . One recognizes that an increase in T_p leads to a faster dielectric relaxation at T_0 . The arrow reflects the loss maximum of hexagonal ice cooled from the liquid state and agrees well with the measurement carried out for $T_p = 270$ K.

from “cubic” to hexagonal ice is not easily recognized. To underscore this statement in Fig. 1(a), we present the results obtained for a sample of ice I that was prepared from deuterated eHDA and heated to 200 K at a rate $|q| = 0.5$ K/min, i.e., to a temperature much above the LDA \rightarrow ice I_c transformation taking place near 160 K. The return temperature $T_0 = 200$ K was chosen for this material because the dielectric loss maximum is then well resolved within the frequency window of our experiments. Afterwards we performed a zig-zag temperature scan with $|q| = 0.4$ K/min as documented in the inset of Fig. 1(a). Successively larger temperature excursions were executed with multiple returns to T_0 . As an illustration of how the dielectric spectra recorded under such conditions typically look like, in Fig. 1(a) we show data obtained upon heating subsequent to reaching T_0 the second time [cycle 2 according to inset of Fig. 1(a)]. One recognizes a smooth temperature evolution of the spectra and that a transition among different ice I states is not obvious.

A clear view of the consequences of the temperature cycling and hallmarks for the cubic to hexagonal transition can be gained from Fig. 1(b). Here we collect dielectric loss spectra that were all acquired at the same temperature 205 K after returning from 210, 230, 250, or 270 K. The spectra taken before and after the first cycle (peak temperature $T_p = 210$ K) are barely distinguishable. That is, hysteresis effects that would signal a transition among different states of ice I are not discernible. This finding suggests that the transition to hexagonal ice has only barely, if at all begun. Thus, one may plausibly assume that spectrum 1 in Fig. 1(b) essentially refers to that of “cubic” ice. For comparison, spectrum 4 recorded for $T_p = 270$ K should refer to that of hexagonal ice. This assumption was confirmed by producing hexagonal ice from the liquid and recording its loss spectrum at 205 K. The loss peak position from this sample is included in Fig. 1(b) (see the arrow) and agrees with that of the ice sample cycled down after reaching 270 K. Spectra 2 and 3 recorded at the end of cycles 2 and 3 are intermediate between the ones of cubic (spectrum 1) and hexagonal ice (spectrum 4). That is, the dielectric dynamics of the ice I sample progress from cubic character toward hexagonal character in cycles 2 and 3. Interestingly, the single-peak character of the loss functions obtained at intermediate T_p 's [spectra 2 and 3 in Fig. 1(b)] reveals that, in harmony with previous observations,¹⁴ the sample is homogeneous in nature and not a mixture of two macroscopic components.

Such a single-process dielectric response is displayed by all of the presently investigated samples. To demonstrate that this feature is shared also for a crystalline mother phase, the Appendix includes similar results obtained for ice I that was produced from ice XII. The key finding is the same in both Fig. 1(b) for HDA and Fig. 7 in the Appendix for ice XII: the dynamics in ice I change progressively from cycle 1 to cycle 4. Most notably, a shift in dynamics is even observed at the return temperature between cycle 3 and cycle 4, when the sample was heated previously to $T_p = 270$ K instead of $T_p = 250$ K.

To obtain an overview of the spectral evolution during the temperature scans, rather than plotting the temperature dependence of *all* spectra, Fig. 2(a) shows $\varepsilon''(T)$ measured

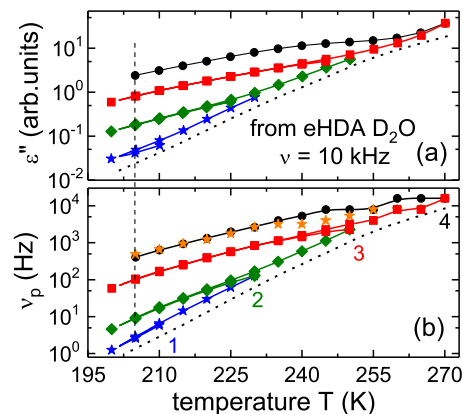


FIG. 2. (a) Dielectric loss of deuterated eHDA recorded at 10 kHz upon cycling the temperature using a rate of $|q| = 0.4$ K/min according to the scheme presented in Fig. 1(a). (b) Temperature variation of the dielectric loss peak frequency ν_p for the same sample and same temperature protocol as in (a). In (b), the orange stars correspond to the measurements for the sample that was melted and subsequently refrozen, and the numbers correspond to the onsets of the cycles as indicated in the inset of Fig. 1(a). The vertical dashed line in (a) and (b) corresponds to the return temperature $T_0 = 205$ K. The dotted curved lines in (a) and (b) are guides to the eye; see the text for details.

at $\nu = 10$ kHz for ice I produced from deuterated amorphous state eHDA. Similar $\varepsilon''(T)$ results corresponding to ice I produced from protonated ice XII are shown in the Appendix in Fig. 8. Scanning up and down in the temperature range from about 200 K to 270 K, the data follow very similar temperature dependences. At a given temperature, the dielectric loss increases cycle by cycle, indicating the hysteresis associated with the progressive conversion from cubic to hexagonal. Upon heating from return temperatures T_0 to peak temperatures T_p and cooling back an enhanced dielectric loss is measured. After each $T_p \rightarrow T_0 \rightarrow T_p$ cycle, the increase in the dielectric loss follows a common temperature trend, as indicated by the envelope plotted as a dotted line in Fig. 2. The underlying dielectric loss “background” covers a range of more than 3 decades between T_0 and the melting point of ice and demonstrates the large dynamic contrast between different states of ice I.

For ice I (from eHDA), apart from showing $\varepsilon''(T)$ in Fig. 2(a), we determined the peak frequencies ν_p from *all* spectra by fitting the loss curves in Fig. 1(a) by a sum of a Havriliak-Negami function³⁹ for the loss peak and a power-law accounting for the low-frequency conductivity

$$\varepsilon'' = \text{Im} \left\{ \Delta\varepsilon [1 + (i\nu/\nu_p)^\alpha]^{-\gamma} \right\} + \sigma_0 / (2\pi\nu). \quad (1)$$

In Eq. (1), $\Delta\varepsilon$ denotes the relaxation strength and σ_0 denotes the dc electrical conductivity. The exponents $\alpha, \gamma < 1$ reflect the broadening in the distribution of dielectric relaxation rates.³⁹ The values of the two parameters vary slightly with the cycle number: from 1 to 4, α changes from 0.95 to 0.8 and γ from 0.8 to 1, respectively. The resulting overall temperature dependence of $\nu_p(T)$, cf. Fig. 2(b), confirms the observations made for $\varepsilon''(T)$ in Fig. 2(a). Clearly, also the peak frequency increases cycle by cycle, reflecting increasingly faster dielectric dynamics as the transition from cubic to hexagonal progresses. Interestingly, for a given cycle, the data points obtained upon cooling practically coincide with those obtained

on reheating. This finding confirms that upon cooling ($T_p \rightarrow T_0$) as well as for the subsequent heating ($T_0 \rightarrow T_p$), the fraction of the irreversibly converted material is preserved. In other words, transformation from cubic toward hexagonal ice is not detectable on the time scale of our investigations at a given temperature. Only ramping the temperature to higher maximum temperatures allows for progression of the transformation from cubic to hexagonal on the time scale of our experiment. The most surprising finding here is that even for maximum temperatures above 250 K, the dynamics continue to change, even if the stacking sequence itself no longer changes above 250 K.

B. Nuclear spin relaxometry

In order to check the surprising dielectric findings reported in Sec. III A by a different experimental method, we carried out NMR experiments in which we measured the deuteron spin-lattice relaxation times, T_1 , of ice I generated from uHDA and from eHDA. Again we used a cycling protocol which, however, had to differ from the one shown in Fig. 1. This is because in some cases, the spin-lattice relaxation times in ice are longer than 1000 s so that a determination of T_1 can take several hours. Therefore, in the NMR study, we implemented the step-like cycling illustrated in Fig. 3. Subsequent to stepping and sufficiently stabilizing the temperature (cf. the arrows in Fig. 3), relaxometry measurements were started. One recognizes that the chosen scheme includes melting, enabling measurement of refrozen hexagonal ice for comparison.

In a first step, let us present longitudinal magnetization recovery curves, $M(t)$, recorded at 200 K from which spin relaxation rates were derived. The corresponding measurements were started subsequent to returning from various temperatures T_p ; see the downward arrows in Fig. 3. The $M(t)$ curves shown in Fig. 4 were acquired by applying the saturation recovery technique and the data could be well described using a Kohlrausch function

$$M(t) = M_0 \{1 - \exp[-(t/T_1)^\mu]\}. \quad (2)$$

Here M_0 denotes the equilibrium magnetization and μ is a stretching exponent. For the curves in Fig. 4, recorded at 200 K after the cooling from T_p , relatively good fits were obtained with an exponent of μ close to 1. One observes that the $M(t)$ curve corresponding to $T_p = 230$ K are not close to nearing

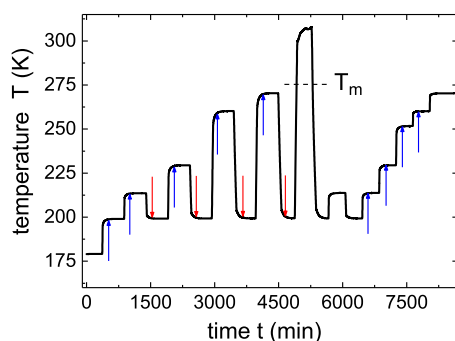


FIG. 3. Cycling scheme used for the NMR measurements. Upward arrows indicate the start of measurements after an upward step in temperature, and downward arrows indicate the start of measurements after a downward temperature step. The dashed line indicates the melting point T_m of ice.

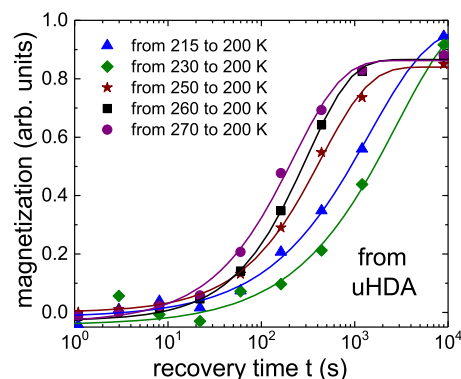


FIG. 4. Deuteron magnetization recoveries of ice I recorded after heating uHDA (cf. the downward arrows in Fig. 3). All measurements were performed at 200 K after returning from higher temperatures T_p . The solid lines are fits using Eq. (2).

saturation even for very long recovery times $t = 10\,000$ s, implying that the determination of T_1 is enormously difficult and not particularly reliable under these circumstances.

For comparison, Fig. 5 (upper scale) summarizes T_1 measurements at T_p on ice I made from uHDA and from eHDA, as well as from hexagonal ice produced by freezing water. Within experimental error, all these data agree with each other and are compared with earlier measurements.^{33,40} Figure 5 reveals that the spin-lattice relaxation rates are strongly temperature dependent, covering a range of almost 3 decades when going from 200 K to near the melting point of ice, similar to the extent of the envelope plotted as dashed line in Fig. 2. Hence, in this respect the behavior of the “background” NMR rates resembles that of the dielectric results.

The relaxation rates $1/T_1$ measured at a return temperature of 200 K (cf. Fig. 4) are summarized in Fig. 5 (lower scale) as a function of the peak temperatures T_p that range from 210 to 270 K.⁴¹ Remarkably, within the significant error bars evident at low temperatures, a return after each cycling leads to a successive increase of $1/T_1$ indicating a dynamical enhancement as the transformation from a state of ice with many stacking faults to hexagonal ice progresses. Including also

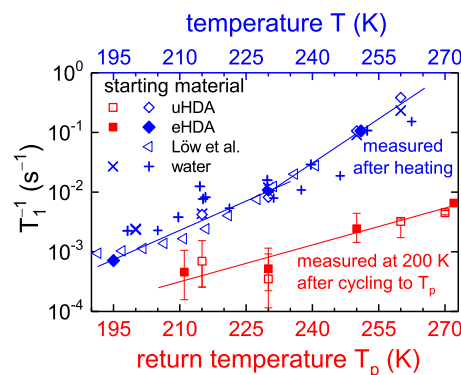


FIG. 5. Spin-lattice relaxation rates of ice I as obtained from various starting materials. The diamonds refer to measurements carried out after stepping the temperatures up to various T_p (upper scale) and the squares refer to experiments performed after cycling the temperature down to $T_0 = 200$ K (lower scale). The data from Löw *et al.*³³ are from a sample with eHDA as mother phase. Rates from (re-) frozen water are from the present work (\times) and from Ref. 40 ($+$). The lines are drawn to guide the eye.

data from a sample generated using eHDA as starting material, it is evident that spin-lattice relaxation depends systematically on the temperature excursion amplitude akin to the observations made in Fig. 1(b) using dielectric spectroscopy. Furthermore, the NMR data indicate that the transformation progresses even when changing the return temperature in the range between 250 K and 270 K.

IV. DISCUSSION

For a close comparison of the NMR data with those from dielectric spectroscopy, by virtue of the fluctuation-dissipation theorem, one may relate the spin-lattice relaxation rate to the imaginary part χ'' of the corresponding normalized dynamic susceptibility via⁴²

$$\frac{1}{T_1} = K[\chi''(\nu_L) + 4\chi''(2\nu_L)]. \quad (3)$$

Here, K denotes the square of the essentially temperature independent deuteron quadrupolar coupling constant.⁴⁰ Neglecting the typically small deviation in the susceptibility probed at frequencies ν_L and $2\nu_L$ and disregarding the slight differences in the orientational sensitivity of dielectric quantities (which depend on rank 1 Legendre polynomials) vs. NMR quantities (referring to rank 2 Legendre polynomials), one arrives at $1/T_1 \propto \varepsilon''(\nu_L)$. This means that by and large, $1/T_1$ can be regarded as a measure of the (dielectric) loss probed at the Larmor frequency, which via $2\pi\nu_L\tau \approx 1$ implies that NMR is sensitive to the dynamics on the nanosecond time scale.

Thus, despite the fact that the NMR and the dielectric data probe the dynamics of ice I on vastly different frequency scales, they show very similar effects. Nevertheless, at the return temperatures, the peak frequencies from the dielectric measurements change by two decades when changing T_p , cf. Fig. 2(a), while the NMR rates—due to their sensitivity not only to molecular reorientation processes but also to lattice vibrations⁴³—vary by only a factor of ten; see Fig. 5. Thus, the large contrast between the incipient and final ice I states suggests that dielectric spectroscopy is better suited than NMR for quantitative analyses aiming at mapping out the relative amount of H₂O displaying hexagonal ice dynamics in our samples.

For the following discussion, one should keep in mind that the X-ray diffraction studies of ice mainly resolve the *structural* correlations within the *oxygen* lattice.⁴⁴ On the other hand, dielectric spectroscopy and deuteron NMR are mainly sensitive to the *dynamics* of the microscopic defects violating the “ice rules” governing the configuration of the *hydrogen* matrix.

The results presently obtained for the hydrogen matrix will be compared in the following with the previous results from the calorimetric studies of the $I_{c(h)} \rightarrow I_h$ transition.^{14,15} The enthalpy change associated with this transition depends on the initial amount of stacking disorder and was found to be rather tiny, in the range -13 J mol^{-1} , from mother-phase ice IX, up to -50 J mol^{-1} from mother-phases ice V and ice VI.¹⁵ Ice I_c produced from liquid water droplets shows a transition enthalpy of -128 J mol^{-1} and two distinct

peaks in the calorigrams that are attributable to the $I_c \rightarrow I_h$ transition.²⁰ The difference in enthalpies was explained by Handa *et al.* in terms of a “formation of ice I_c with a substantial fraction of stacking faults, the formation of regular stacking variants that are intermediate between ice I_h and I_c , a transformation of ice I_c to I_h that releases some of its heat too slowly to detect, and formation of ice I_c having grains that are small enough,” even though no direct evidence for stacking faults in ice I_c even existed at the time.¹⁵

In the studies above the term “stacking” refers to the oxygen lattice. On the other hand, we suggest that our study monitors the evolution of the stacking faults as reflected by the dynamics of the hydrogen network. Nevertheless, observations similar to the ones mentioned above by Handa *et al.*, namely (i) “transformation. . . too slowly to detect”¹⁵ and (ii) an assortment of “grains. . . small enough,”¹⁵ can be also inferred from the current data. Concerning point (ii), the nature of a homogeneous, microscopic/mesoscopic disorder implies that properties such as those accessible using dielectric spectroscopy or spin relaxometry will not lead to a mere superposition of loss spectra or NMR recovery curves originating from “hexagonal” and “non-hexagonal” components. Such components should manifest themselves as two separable contributions similar to a macroscopic phase separation. Neither in the dielectric loss data, cf. Fig. 1(b), nor in the magnetization buildup curves (Fig. 4) is such a kind of large-scale heterogeneity observed. Obviously, the temperature induced change of the stacking disorder leads to a merely continuous change in the spin-relaxation rate or the dielectric peak frequency from which information about the stacking arrangement should be accessible.

In relation to point (i), we note that, irrespective of the structural details of the mother-phase and the hydrogen isotope, the data sets in Fig. 2 (and those presented in the Appendix) allow for a remarkable observation: During each $T_p \rightarrow T_0 \rightarrow T_p$ cycle, the relaxation behavior is highly reproducible. This suggests that kinetic effects need not be considered for a description of the dielectric results regarding the underlying change in ice I.

The peak frequency from melt-produced hexagonal ice, cf. the arrow in Fig. 1(b) and the orange stars in Fig. 2(b), agrees with that from cycle 4 in which eHDA/D₂O was used as mother phase. This observation indicates that after this cycle, the transition to hexagonal ice-like dynamics is complete. Conversely, in view of the substantial efforts necessary in studies aiming at producing “pure” cubic ice,⁴⁵ it is clear that the “cubic” ice emerging from all currently investigated mother-phases, even at the lowest temperatures at which ice “ I_c ” occurs, contains a significant (but unknown) amount of stacking faults. As the sample produced from ice XII demonstrates, see Figs. 7 and 8 in the Appendix, the conversion toward the neat hexagonal phase becomes significant only for temperatures exceeding 200 K. At each investigated temperature, we will now estimate a non-converted fraction $X(T)$ of the material which has not yet irreversibly transformed to hexagonal ice. We refrain from using the scattering-based¹⁴ term “cubicity” for this dynamics-derived quantity, in order to indicate that our determination is entirely different from that defined on the basis of diffraction experiments.

As suggested by the vertical dashed line in Fig. 2(b), one may base the assessment of $X(T)$ on the dielectric relaxation rate by interpolating between the limiting ends so that

$$X(T) = \frac{\log \nu(T) - \log \nu_c}{\log \nu_h - \log \nu_c}. \quad (4)$$

Here the indices c and h refer to the limiting cases of “cubic” or hexagonal stacking, respectively. The definition in Eq. (4) implies that $X(T) \rightarrow 1$ at small temperatures which, also in light of the above remarks, should not be taken to indicate that the “cubic” fraction is 1 but that it is at its (unknown) maximum.

For the samples produced from eHDA or from ice XII, the evaluation of X yields very similar results, see Fig. 6, that barely depend on whether the mother phases are protonated or deuterated. For these materials, one may say that the indices c and h in Eq. (4) refer to peak frequencies determined at temperatures of T_0 (180 K and 205 K for the materials produced from ice XII and eHDA, respectively) and an upper temperature of about 270 K.

This suggests that residuals of the non-hexagonal state eventually converting to hexagonal ice remain present until just below the melting point. In this respect, the hydrogen network reaches its equilibrium state only at much higher temperatures than the oxygen lattice does. This finding may rationalize the small enthalpy change and the unusual, two-steps calorimetric signature associated with the $I_c \rightarrow I_h$ transition.¹⁵

Interestingly, for all of the samples shown in Fig. 6, in the entire investigated temperature range up to 270 K, the dynamics of the intermediate state remain slower than that of neat I_h . The latter observation is in harmony with previous results obtained in a more restricted temperature range.³¹ The impact of planar (stacking) defects on the dynamics of hexagonal ice (which obviously slows the dynamics) is thus different from the impact of orientational and ionic point defects in crystalline ices which enhance (rather than inhibit) the dynamics if suitable dopants are used.⁴⁶ This includes the doping with HCl of several high-density ice phases^{47,48} as well as KOH-doped cubic ice I_c .³⁰ In all these cases, the relaxation dynamics on, e.g., a millisecond time scale, take place at lower temperatures than for the undoped ices that are discussed here.

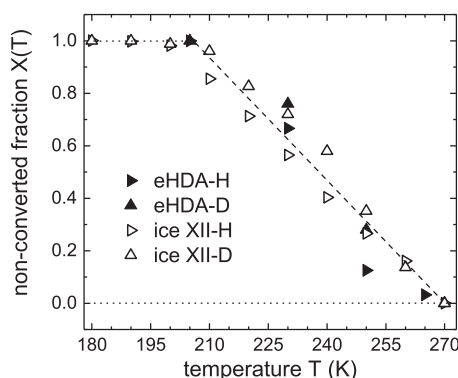


FIG. 6. Normalized fraction of ice I that has not converted to the hexagonal form as determined via dielectric spectroscopy [see Eq. (4) and text for details]. The letters “H” and “D” in the upper right legend refer to protonated and deuterated materials, respectively. The two horizontal dotted lines mark the normalization limits and the dashed lines are guides to the eye.

Previous investigations of the transformation from eHDA to LDA, taking place above the glass transition of the former, indicated that it is not affected by doping.⁴⁹ This finding corroborates the notion that the eHDA \rightarrow LDA transformation is *not* of the crystal-to-crystal type. In this regard by future measurements, it would be interesting to check whether or not the characteristic temperature at which the presently investigated crystal-to-crystal dynamical transition occurs can be tuned by the addition of suitable dopants.

V. CONCLUSIONS

In the present article, we analyzed the dynamic aspects accompanying the transformation of “cubic” ice to hexagonal ice by means of dielectric spectroscopy and NMR. The most important finding is that the experiments probing the rearrangements of the hydrogen matrix are sensitive to dynamical changes apparently initiated by stacking disorder. Based on temperature cycling scans, we find that these rearrangements are not complete until temperatures up to near the melting point are reached. This gradual transition toward the dynamics of neat hexagonal ice displays several remarkable characteristics:

- (i) it extends over a broad range of about 70 K,
- (ii) it is independent of the use of deuterium or hydrogen isotopes and of the tested mother phases (eHDA, uHDA, and ice XII) from which cubic ice is produced,
- (iii) at a given temperature, it does not exhibit any signs of kinetics on the time scale of the present experiments,
- (iv) it depends on the physical characteristics of the hydrogen rather than the oxygen matrix,
- (v) it vanishes once the sample is melted and then refrozen, and
- (vi) the dynamics are always faster in hexagonal ice than in stacking-faulty cubic ice.

The dielectric and NMR data also reveal that the intermediate state of ice I state does not consist of two macroscopically separated components, e.g., one being already converted to hexagonal ice and the other one not. Instead, akin to the stacking disorder that characterizes the oxygen lattice, the hydrogen lattice displays a state that is homogeneous on microscopic and mesoscopic scales.

ACKNOWLEDGMENTS

We thank the Deutsche Forschungsgemeinschaft, Grant No. BO1301/12-1 and the Austrian Science Fund FWF, Project No. I1392, for the financial support provided for this project. Thomas Loerting thanks the Alexander von Humboldt Foundation for the financial support of his research visit in Dortmund. V.F.L. is a recipient of a DOC fellowship of the Austrian Academy of Sciences ÖAW.

APPENDIX: DIELECTRIC RESPONSE OF ICE I PRODUCED FROM PROTONATED ICE XII

As observed in Fig. 7, the evolution of the dielectric response of ice I produced from protonated ice XII at the return temperature is similar to the one exhibited by ice I produced from deuterated HDA, Fig. 1(b).

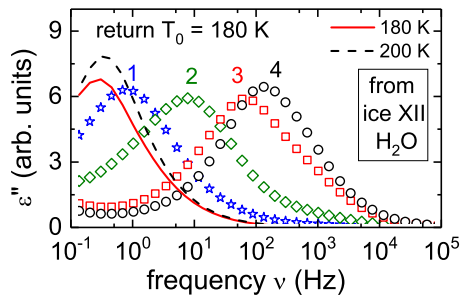


FIG. 7. Dielectric loss measurements on ice I obtained from protonated ice XII analogous to those shown in Fig. 1(b) for the deuterated HDA material. The spectra were acquired at a return temperature $T_0 = 180$ K after cooling the sample down from the peak temperatures $T_p = 210, 230, 250,$ and 260 K. The small change in the peak position for the spectra recorded at 180 K and at 200 K demonstrates that for $T < 200$ K no major dynamic variations occur.

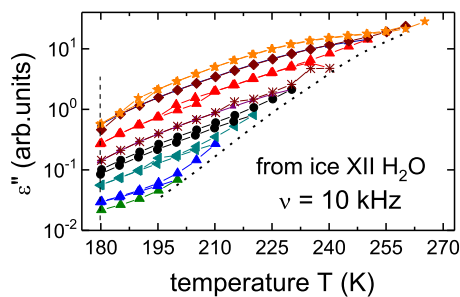


FIG. 8. Dielectric loss at 10 kHz for ice I obtained from protonated ice XII, recorded upon cycling the temperature with $|q| = 0.6$ K/min.

The main procedural differences with respect to the situation presented in Fig. 1(b) are that here the maximum peak temperature T_p is 260 K and that the return temperature is $T_0 = 180$ K. The lower temperature T_0 at which all spectra in Fig. 7 were recorded rationalizes why for identical T_p the overall dynamics appear to be somewhat slower for ice I derived from ice XII as the mother phase than for ice I derived from eHDA in Fig. 1(b).

Figure 8 shows that the dielectric loss data at 10 kHz for ice I produced from protonated ice XII also follow a similar temperature dependence as those corresponding to the deuterated HDA as precursor, see Fig. 2(a). The underlying “background” loss, highlighted by the dotted curved line in Fig. 8, covers a similar range as in the HDA case, see Fig. 2(a).

- ¹E. Whalley and G. E. McLaurin, *J. Opt. Soc. Am. A* **1**, 1166 (1984).
- ²M. Riikonen, M. Sillanpaa, L. Virta, D. Sullivan, J. Moilanen, and I. Luukkonen, *Appl. Opt.* **39**, 6080 (2000).
- ³L. Lupi, A. Hudait, B. Peters, M. Grünwald, R. Gotchy Mullen, A. H. Nguyen, and V. Molinero, *Nature* **551**, 218 (2017).
- ⁴A. J. Weinheimer and C. A. Knight, *J. Atmos. Sci.* **44**, 3304 (1987).
- ⁵N. A. Lefaudeux, *Appl. Opt.* **50**, F121 (2011).
- ⁶B. J. Murray, C. G. Salzmann, A. J. Heymsfield, S. Dobbie, R. R. Neely III, and C. J. Cox, *Bull. Am. Meteorol. Soc.* **96**, 1519 (2015).
- ⁷G. P. Johari and O. Andersson, *J. Chem. Phys.* **143**, 054505 (2015).
- ⁸J. E. Shilling, M. A. Tolbert, O. B. Toon, E. J. Jensen, B. J. Murray, and A. K. Bertram, *Geophys. Res. Lett.* **33**, L17801, <https://doi.org/10.1029/2006gl026671> (2006); A. Bogdan and T. Loerting, in *Geophysical Research Abstracts* (EGU, 2009), Vol. 11, EGU2009-13419.
- ⁹D. M. Murphy, *Geophys. Res. Lett.* **30**, 2230, <https://doi.org/10.1029/2003GL018566> (2003).
- ¹⁰A. Kouchi and T. Kuroda, *Astrophys. Space Sci. Libr.* **173**, 87 (1991).
- ¹¹P. Jenniskens and D. F. Blake, *Science* **265**, 753 (1994).

- ¹²T. C. Hansen, C. Sippel, and W. F. Kuhs, *Z. Kristallogr.-Cryst. Mater.* **230**, 75 (2015).
- ¹³T. L. Malkin, B. J. Murray, C. G. Salzmann, V. Molinero, S. J. Pickering, and T. F. Whale, *Phys. Chem. Chem. Phys.* **17**, 60 (2015).
- ¹⁴W. F. Kuhs, C. Sippel, A. Falenty, and T. C. Hansen, *Proc. Natl. Acad. Sci. U. S. A.* **109**, 21259 (2012).
- ¹⁵Y. P. Handa, D. D. Klug, and E. Whalley, *Can. J. Chem.* **66**, 919 (1988).
- ¹⁶H. König, *Z. Kristallogr.-Cryst. Mater.* **105**, 279 (1943).
- ¹⁷L. G. Dowell and A. P. Rinfret, *Nature* **188**, 1144 (1960).
- ¹⁸T. Hondoh, *Philos. Mag.* **95**, 3590 (2015).
- ¹⁹W. F. Kuhs, G. Genov, D. K. Staykova, and T. Hansen, *Phys. Chem. Chem. Phys.* **6**, 4917 (2004).
- ²⁰I. Kohl, E. Mayer, and A. Hallbrucker, *Phys. Chem. Chem. Phys.* **2**, 1579 (2000).
- ²¹J. E. Bertie and E. Whalley, *J. Chem. Phys.* **40**, 1637 (1964).
- ²²J. E. Bertie, H. J. Labbe, and E. Whalley, *J. Chem. Phys.* **10**, 4501 (1969).
- ²³T. H. G. Carr, J. J. Shephard, and C. G. Salzmann, *J. Phys. Chem. Lett.* **5**, 2469 (2014).
- ²⁴E. Mayer and A. Hallbrucker, *Nature* **325**, 601 (1987).
- ²⁵T. L. Malkin, B. J. Murray, A. V. Brukhno, J. Anwar, and C. G. Salzmann, *Proc. Natl. Acad. Sci. U. S. A.* **109**, 1041 (2012).
- ²⁶W. F. Kuhs, D. V. Bliss, and J. L. Finney, *J. Phys. Colloq.* **48**, C1-631 (1987).
- ²⁷T. C. Hansen, A. Falenty, and W. F. Kuhs, in *Symposium on the Physics and Chemistry of Ice, Physics and Chemistry of Ice*, edited by W. F. Kuhs (Royal Society of Chemistry, Cambridge, 2007), pp. 201–208.
- ²⁸T. C. Hansen, M. M. Koza, and W. F. Kuhs, *J. Phys.: Condens. Matter* **20**, 285104 (2008).
- ²⁹T. C. Hansen, M. M. Koza, P. Lindner, and W. F. Kuhs, *J. Phys.: Condens. Matter* **20**, 285105 (2008).
- ³⁰O. Yamamuro, M. Oguni, T. Matsuo, and H. Suga, *J. Phys. Chem. Solids* **48**, 935 (1987).
- ³¹S. R. Gough and D. W. Davidson, *J. Chem. Phys.* **52**, 5442 (1970).
- ³²O. Haida, T. Matsuo, H. Suga, and S. Seki, *J. Chem. Thermodyn.* **6**, 815 (1974).
- ³³F. Löw, K. Amann-Winkel, B. Geil, T. Loerting, C. Wittich, F. Fujara, *Phys. Chem. Chem. Phys.* **15**, 576 (2013). The measurements reported in that article were obtained at a Larmor frequency of 46.1 MHz.
- ³⁴K. Amann-Winkel, C. Gainaru, P. H. Handle, M. Seidl, H. Nelson, R. Böhmer, and T. Loerting, *Proc. Natl. Acad. Sci. U. S. A.* **44**, 17720 (2013).
- ³⁵H. Nelson, S. Schildmann, A. Nowaczyk, C. Gainaru, B. Geil, and R. Böhmer, *Phys. Chem. Chem. Phys.* **15**, 6355 (2013).
- ³⁶O. Mishima, L. D. Calvert, and E. Whalley, *Nature* **310**, 393 (1984).
- ³⁷K. Winkel, D. T. Bowron, T. Loerting, E. Mayer, and J. L. Finney, *J. Chem. Phys.* **130**, 204502 (2009).
- ³⁸C. G. Salzmann, T. Loerting, I. Kohl, E. Mayer, and A. Hallbrucker, *Can. J. Phys.* **81**, 25 (2003); I. Kohl, T. Loerting, C. Salzmann, E. Mayer, and A. Hallbrucker, in *New Kinds of Phase Transition: Transformation in Disordered Substances*, edited by V. V. Brazhkin, S. V. Buldyrev, V. N. Ryhkov, and H. E. Stanley (Kluwer Academic Publishers, 2002), pp. 325–333.
- ³⁹S. Havriliak and S. Negami, *J. Polym. Sci., Part C: Polym. Symp.* **14**, 99 (1966).
- ⁴⁰B. Geil, T. M. Kirschgen, and F. Fujara, *Phys. Rev. B* **72**, 014304 (2005). The measurements reported in that article were obtained at Larmor frequencies of 55 and 50 MHz.
- ⁴¹Naively, one would expect that the $1/T_1$ rates measured at 200 K after cycling to just below the melting point (referring to the lower scale in Fig. 5) should coincide with the measurements of hexagonal ice produced from refrozen water (see the \times at 200 K in Fig. 5). However, our experimental data show that refreezing reduces the $1/T_1$ rate by a factor of about 2. For instance, when comparing the data on ice and refrozen water (cf. diamonds and crosses in Fig. 5) $1/T_1$ deviations of up to a factor of 1.5 are seen. To rationalize any remaining potential discrepancy we draw attention to results by F. Löw and F. Fujara, private communication, 2014. These authors have shown that near 200 K a rate reduction by a factor of 2 can be achieved by decreasing the level of HCl impurities, e.g., from 10^{-6} to 10^{-5} mol. % (or over a correspondingly smaller span if a factor of less than 2 is to be explained), it is suggestive that refreezing expels minute amounts of impurities that may have been present in the uHDA mother phase.
- ⁴²T. Blochowicz, A. Kudlik, S. Benkhof, J. Senker, E. Rössler, and G. Hinze, *J. Chem. Phys.* **110**, 12011 (1999).
- ⁴³This statement that toward lower temperature contributions from lattice vibrations are increasingly enhancing the measured $1/T_1$ is corroborated by

the observation that near 200 K the $1/T_1$ rates measured before cycling are larger than expected from a simple extrapolation of the data taken at higher temperatures.

⁴⁴At this point, it is worth mentioning that our T -dependent X-ray investigations (not shown) of eHDA/D₂O are consistent with the results from Ref. 19 in the sense that they reveal that the fingerprints of the cubic arrangements vanish for temperatures above 240 K.

⁴⁵P. Geiger, C. Dellago, M. Macher, C. Franchini, G. Kresse, J. Bernard, J. N. Stern, and T. Loerting, *J. Phys. Chem. C* **118**, 10989 (2014).

⁴⁶V. F. Petrenko and R. W. Whitworth, *Physics of Ice* (University Press, Oxford, 1999).

⁴⁷K. W. Köster, V. Fuentes-Landete, A. Raidt, M. Seidl, C. Gainaru, T. Loerting, and R. Böhmer, *Nat. Commun.* **6**, 7349 (2015), also see Erratum (to be published).

⁴⁸K. W. Köster, A. Raidt, C. Gainaru, V. Fuentes-Landete, T. Loerting, and R. Böhmer, *Phys. Rev. B* **94**, 184306 (2016).

⁴⁹S. Lemke, P. H. Handle, L. Plaga, M. Seidl, V. Fuentes-Landete, K. Amann-Winkel, K. W. Köster, C. Gainaru, T. Loerting, and R. Böhmer, *J. Chem. Phys.* **147**, 034506 (2017).